THE JOURNAL OF PHYSICAL CHEMISTRY C
A JOURNAL OF THE AMERICAN CHEMICAL SOCIETY

pubs.acs.org/JPCC
Article

Metastability Limit of Hydrated Phases of Sodium Sulfate under Temperature Cycling for Heat Storage

Anne Claude, Rosa Sinaasappel, Jorik van de Groep, and Noushine Shahidzadeh*

Cite This: J. Phys. Chem. C 2026, 130, 3721−3729
Read Online

ACCESS | Metrics & More | Article Recommendations | Supporting Information

ABSTRACT: Sodium sulfate is an inexpensive, earth-abundant salt with great potential for heat storage applications due to its high energy density. Phase transitions involving crystallization of sodium sulfate decahydrate (Na_2SO_4•$10H_2O$, mirabilite) are accompanied by a large latent heat. Using laser-transmittance, confocal Raman microspectroscopy, and freezing experiments, we accurately define the dissolution and metastability lines of the heptahydrate (Na_2SO_4•$7H_2O$) and decahydrate phases, and subsequently present the complete phase diagram of the binary system Na_2SO_4−water. The metastable zone width (MSZW) is found to be independent of concentration, in the range of $\Delta T \sim 17$ °C for the heptahydrate, and $\Delta T \sim 40$−46 °C for the decahydrate form. The latter phase can directly precipitate only from an undersaturated solution below 1.4 mol/kg at a temperature below 0 °C, as in this range of concentrations the metastability line of the heptahydrate phase passes behind that of mirabilite at lower temperatures. Its precipitation is however found not to be ice-assisted, as the decahydrate phase precipitates before ice following the experimentally defined MSZW. Lastly, at high salt concentrations (>1.4 mol/kg), we show that the addition of various types of impurities into salt solutions has no significant impact on the reduction of the activation energy barrier of mirabilite to bypass the formation of the heptahydrate with a lower energy density.

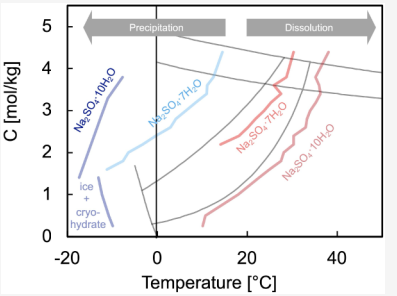

1. INTRODUCTION

Heating represents almost 70% of household energy consumption, including water heating and space heating.[1] In 2022, 63% of this heat was produced by fossil fuels (oil, natural gas, and coal).[2] The International Energy Agency predicts a reduction in the use of fossil fuels of ∼20% by 2030, which is assuredly not sufficient to achieve carbon neutrality in 2050, as targeted in the European Climate Law.[3] Therefore, there is an urgent need to find sustainable alternatives to decarbonize heating by using heat pumps, solar thermal systems, as well as Phase Change Materials (PCM)[4,5] as thermal batteries.

A particular type of PCM, namely hydrated salts (M_pX_q•mH_2O), is a promising material for domestic heat storage[6,7] by virtue of their high energy density, which ranges between 1 and 3 GJ/m,[3] comparable to that of lithium-ion batteries (0.46−0.72 MJ/kg, or between 0.72 and 1.8 GJ/m,[3]).[8−11] By leveraging the reversible (de)hydration reaction or dissolution/precipitation, these hydrated salts can provide cooling by absorbing heat during warm environmental periods and reversibly release latent heat during colder periods.

Despite their promise, the deployment of these crystalline materials in sustainable thermal batteries is still hindered by challenges, including limited reproducibility, supercooling, as well as undesired and irreversible phase transformations leading to their degradation over several temperature cycles.[12,13] Some compounds exhibit polymorphism, with multiple hydrated crystalline phases and different crystalline structures. In addition, the microcrystallite size of the salt is also clearly important for the speed and efficiency of (de)hydration steps. Since the selective use of phase transitions for thermal energy storage relies on the temperature dependence of a salt's solubility line, the accuracy of the phase diagram is thus crucial to determine the temperature conditions at which hydration or dehydration occurs, as well as the number of possible hydration transitions for a given salt.

Among all the hydrated salts, sodium sulfate is particularly interesting, as it is an inexpensive, earth-abundant salt with a high energy density. Indeed, this system has four phases: two anhydrous phases—(Na_2SO_4) *thenardite III (metastable) and thenardite V* (stable)—and two hydrates—the stable decahydrate (Na_2SO_4•$10H_2O$, latent heat ∼0.24 MJ/kg[14]) also known as *mirabilite* or *Glauber's salt*, and the metastable heptahydrate (Na_2SO_4•$7H_2O$, latent heat ∼0.088 MJ/kg[15]). For thermal energy storage applications, the formation of mirabilite is most desirable, as its energy density is around 2.7 times higher than that of the heptahydrate. The equilibrium phase diagram of a Na_2SO_4−H_2O system, as defined by the Pitzer model[16] (Figure 1), shows the different phases by featuring lines representing solubility limits and freezing points, and regions denoting which phases coexist at equilibrium.

Received: November 27, 2025
Revised: February 3, 2026
Accepted: February 4, 2026
Published: February 27, 2026

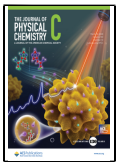

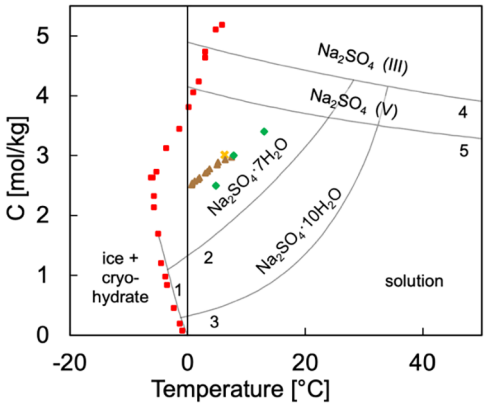

Figure 1. Equilibrium phase diagram of Na_2SO_4−H_2O system and supersolubility lines of the heptahydrate phase during thermal cycling reported in the literature. In gray, Steiger et Asmussen (2008) represents equilibrium solubility lines of all the phases derived from calculations with Pitzer's model: (1) freezing of ice and sodium sulfate decahydrate, equilibrium solubility lines of (2) sodium sulfate heptahydrate (metastable phase), (3) sodium sulfate decahydrate, (4) thenardite III (metastable phase), and (5) thenardite V. The points on the phase diagram represent the data of the supersolubility curves obtained by Hartley et al.[21] (1908, ■), Balarew et al.[23] (2017, ▲), Derluyn et al.[18] (2011, ♦), and Denecker et al.[22] (2014, ×), except the ■ points below 2.5 mol/kg, which are the data of supersolubility for the freezing of the solution, i.e., the domain where ice and sodium sulfate decahydrate coexist.

At the same time, various early experimental works reported in the literature[15−23] show how kinetically driven crystallization can lead to discrepancies with the theoretical equilibrium phase diagram, as (1) nucleation is subjected to a large supercooling; (2) the metastable heptahydrate has been reported to precipitate, even though, based on the prediction, the formation of the decahydrate phase should be energetically more favorable. These results, summarized in Figure 1 and Table 1 explore only narrow ranges of concentrations[21,23] and do not provide insights to explain the two key discrepancies discussed above. These discrepancies, and the challenge of controlling the formation of the desired hydrated phase, are detrimental to heat storage applications; for example, the amount of heat that the heptahydrate salt can store and release remains comparably low.

In this article, we employ precisely controlled thermal-cycling experiments over a wide range of concentrations to demonstrate a revised and complete equilibrium phase diagram of the Na_2SO_4−H_2O system by experimentally pinpointing the solubility and supersolubility (metastability limit) lines of the heptahydrate and decahydrate phases. Our results show that upon heating, the dissolution lines of the heptahydrate and decahydrate phases of sodium sulfate match their equilibrium theoretical solubility lines, while upon cooling, the crystallization (precipitation) lines from the salt solution shift to much lower temperatures. The experimental *metastable zone width* (MSZW)—that is, the temperature interval at a given concentration between the dissolution curve and the precipitation line[24,25]—is found to be independent of concentration, with $\Delta T \sim 40-46$ °C for mirabilite and $\Delta T \sim 17$ °C for the heptahydrate form. Using visual and thermal tracking during freezing experiments at macroscopic and microscopic scales, we show that direct mirabilite precipitation and growth, which occur below 0 °C, are not ice-assisted as was previously reported in the literature.[15] Finally, the presence of various solid particles and micellar colloidal additives with the aim of instigating the precipitation of mirabilite is investigated. Our results surprisingly show no effect of additives on the reduction of the activation energy for the precipitation of mirabilite and the subsequent MSZW upon cooling and heating. Further investigation is needed to explore other nucleation techniques to promote controlled direct formation of the stable hydrate with a narrow MSZW, making it suitable for thermal battery applications.

This study highlights one of the main challenges of hydrated salts applied to thermal energy storage: the undesired supercooling of the system before crystallization occurs, which is difficult to control. Our results show that heterogeneous nucleation is not always the preferred way to promote rapid nucleation and bypass metastable phases. The large variety of impurities tested and proven ineffective inspired us to consider the structure of the liquid as a key factor in the crystallization process. Besides, our results complete the knowledge of the phase diagram of sodium sulfate as we screen it over a wide range of concentrations.

2. EXPERIMENTAL SECTION

2.1. Solution Preparation

Solutions of sodium sulfate below the saturation of thenardite (between 0.25 and 3.4 mol/kg) are prepared at 19 ± 1 °C by weighing 25 g of Millipore water (ρ = 18.2 MΩ cm) and adding the corresponding mass of thenardite (anhydrous Na_2SO_4, Fisher Scientific, >99.5%) in a glass bottle. Each bottle is shaken and heated at 50 °C until complete dissolution of the mirabilite. Then, for each concentration, 4 vials suitable for the Crystal16 tool are filled with 1 mL of solution using a micropipette. For concentrations above the saturation of thenardite, the splitting of the mother solution is no longer possible because of the presence of undissolved solute. Therefore, solutions above 3.4 mol/kg are prepared directly in the 1 mL vials (4 samples per concentration). The same solutions are used for the freezing experiments.

To study the influence of impurities on the crystallization of sodium sulfate, several types of impurities with different chemical compositions, roughnesses, and in different proportions are tested. Rough and angular particles are more suitable to initiate heterogeneous nucleation. For the spherical particles, we try Dynoseed-TS40 beads (polystyrene beads, 20 μm, Microbeads AS) and glass beads (SiO_2, 30−50 μm, Polysciences). For the angular particles, we tested sand (SiO_2 from Zandvoort beach). We also try to use another hydrated salt, namely calcium sulfate: pure plaster powder

Table 1. Previous Experimental Conditions Reported in the Literature on the Supersolubility of Sodium Sulfate Heptahydrate Compared to Our Study

Authors	Hartley et al. (1908)[21]	Balarew et al. (2017)[23]	Derluyn et al. (2011)[18]	Denecker et al. (2014)[22]	Our work
Cooling ramp	0.05 °C/min	1 °C/min	0.13 °C/min	0.25 °C/min	1 °C/min
Sample volume	∼0.6−10 mL	20 mL	50−100 μL	2 mL	1 mL
Stirring rate	Gentle stirring	No info	No stirring	No stirring	800 rpm
Concentration range	2.6−10.6 mol/kg	2.5−3 mol/kg	2.5−3 mol/kg	3 mol/kg	0.2 − 4.4 mol/kg

https://doi.org/10.1021/acs.jpcc.5c08083
J. Phys. Chem. C 2026, 130, 3721−3729

(anhydrous $CaSO_4$, Paris plaster), and gypsum $CaSO_4 \bullet 2H_2O$ (prepared by wetting and drying plaster), which exhibit very sharp tips. This hydrated salt is chosen as it contains the same anion of the salt that we want to form (which could act as a template for the nucleation) and because of its very low solubility, so that it will remain solid in the solution during the heating phases. Preliminary tests are performed for various concentrations (1.4−4.39 mol/kg) and various proportions of particles (wt. 0.6, 3, and 9% by comparison to the mass of thenardite added at the beginning), showing no significant change in the crystallization of sodium sulfate over the entire concentration range. In this paper, we show the results for a 2.8 mol/kg solution of sodium sulfate with wt. 0.6% for all the particles mentioned previously.

In the same vein, we prepare a solution of sodium sulfate at 2.8 mol/kg, containing surfactants above their Critical Micellar Concentration (CMC): 1 mM for CTAB and 10 mM for SDS.

2.2. Thermal Cycling

Thermal energy storage is mimicked by performing thermal cycles using a Crystal16 tool from Technobis. The setup contains four reactors, each with 1 mL vials. All of the samples are stirred magnetically at 800 rpm. For each concentration of sodium sulfate, we perform five cycles of a cooling step (1) followed by a heating step (2), in a row (step 1:50 °C → T_{min}; step 2: T_{min} → 50 °C). The experiments are repeated for two minimal temperatures T_{min} at −5 and −20 °C. The ramp of heating/cooling is fixed at ±1 °C/min and a stay of one h is chosen at each maximal and minimal temperature. Each experiment of five cycles takes roughly 1 day, and in total, more than 150 experiments are performed to systematically map the phase diagram. Additionally, we performed a control experiment over 36 cycles to assess the stability of long-term cyclization, revealing no difference between results after 5 and 36 cycles (Figure S1c).

2.3. Determination of Metastability (Precipitation) Line and Dissolution Line

During the thermal cycling, each vial is illuminated by a laser with a 620 nm wavelength (one source per vial), whose transmission signal is collected on a photodiode connected to a computer. A measurement of the relative transmissivity (difference between the incident light intensity and the intensity after crossing the vial) is taken every second during the thermal cycling. When the transmissivity drops abruptly to 0% (±5%), the sensor does not receive any signal, which means that the light is scattered by the solutes formed in the vial when a high enough supersaturation is reached in the solution. On the contrary, when transmissivity rises to near 100%, all the incident light can be transmitted to the sensor, which means that the solution is completely clear and all the solute is dissolved. Using this approach, we can define, respectively, the temperatures of precipitation and dissolution of the hydrated crystals of sodium sulfate. A calibration for the transmissivity measurement is necessary and is realized within each sample after heating the sample for 1 h at 50 °C, upon which all the solutes are dissolved. This defines the transmissivity at 100%.

2.4. Macroscale Freezing Experiments

A climatic chamber KWP 240 Weiss (called a freezer in this remainder) equipped with a built-in temperature control system Eurotherm 2404, is used to reproduce the experiments of the Crystal16 (without stirring) to provide a visual perspective on the crystallization process *in situ*. Beforehand, we check that stirring does not have any influence on the crystallization of the solution upon cooling (see Figure S1b). The temperature on the outside of the vials is measured by Voltcraft PL-125-T2 USB VS temperature probes, whose tip is preliminarily dipped in thermal paste in order to prevent discrepancy with the temperature in the solution. The probe and thermal paste are then fixed to the side of the vial using Teflon tape. The samples are placed in the freezer before setting the ambient temperature of the freezer to −25 °C, which corresponds to −18 ± 1 °C on the glass of the vial. The ramp of cooling cannot be controlled but ranges between 0.5 and 2 °C/min. A digital camera (Nikon D5300) is used to frame the samples every 10 s, and two Light Emitting Diode (LED) panels are placed at the back of the climate chamber and under the samples to provide a better contrast. We perform these experiments for three concentrations (1.4, 2.8, and 3.8 mol/kg). All of the samples are sealed with parafilm to prevent evaporation of the solution during cooling.

2.5. Microscale Freezing Experiments

Squared glass microcapillaries (0.4 × 4 mm) are filled with pure water and others with a sodium sulfate solution of 1.4 mol/kg and cooled until freezing of the solution using a Peltier element. The capillaries are continuously tracked using a camera (Basler ace acA2040−90um) at 16 and 20 fps (for water and the salt solution, respectively) to follow *in situ* the precipitation of the crystals in the microcapillaries. They are also tracked at different stages of the process under an inverted Leica DM-IRB optical microscope attached to a computer with PixelLink software.

2.6. Raman Confocal Microspectroscopy Characterization

Samples upon cooling are analyzed right after crystal precipitation using Raman confocal spectroscopy. When we take them out of the Crystal16, the samples are exposed to room temperature (19 ± 1 °C), which initiates their dissolution/melting, which makes the acquisition time sensitive. The analysis of the crystals within the vials is performed using a WITec Alpha 300 R microscope coupled to a CCD camera (Andor, Newton EMCCD, DU970P-BVF-355). The heptahydrate sodium sulfate is very sensitive to its environment. In fact, merely with a metallic spatula, it induces mirabilite precipitation. Therefore, all of the spectra were taken directly in the vial, without opening the lid. The laser wavelength used is 532 nm, aligned with a silicon reference sample and a grating with 1800 lines/mm to be able to distinguish the first vibration frequency υ_1 of the sulfate between the heptahydrate and decahydrate forms (988 and 989 cm^{-1} respectively (see Figure S2). For each sample, we took 4 single spectra and images. The spectra provide information about a local point.

2.7. Scanning Electron Microscopy

The SEM images of the additives used as impurities to induce heterogeneous nucleation are taken on a HITACHI TM 3000.

3. RESULTS AND DISCUSSION

3.1. Spontaneous Formation of Sodium Sulfate Heptahydrate

3.1.1. Thermal Cycling between 50 °C and −5 °C. We experimentally investigate phase transitions between the crystal precipitation and dissolution temperatures within a bulk sodium sulfate solution over a wide range of concentrations.

First, we employ thermal cycling of salt solutions starting from 50 °C and cooling down to −5 °C before heating back up. We perform up to five thermal cycles in each experiment, each of which employs 16 reactors simultaneously, while we track the optical transmission *in situ* to identify the temperatures at which crystals precipitate and dissolve (see methods). This offers the ability to measure identical concentrations over many thermal cycles and different concentrations, which provides the crucial quantification of the statistical variations that underlie crystallization events. In addition, using Raman microspectroscopy and optical microscopy, we identify the structural phase of the precipitated crystals at various concentrations.

Figure 2a shows the equilibrium phase diagram from Steiger and Asmussen,[16] with our precipitation line (in blue) superimposed, upon cooling to a minimum temperature of −5 °C. This precipitation line lies far below the equilibrium solubility line of the heptahydrate phase (−13 ± 1 °C). The precipitated crystals in the vials (Figure 2b) show a Raman peak at 988 cm^{-1} characteristic of the heptahydrate form of sodium sulfate (Figure S2); in addition, the morphology of the

https://doi.org/10.1021/acs.jpcc.5c08083
J. Phys. Chem. C 2026, 130, 3721−3729

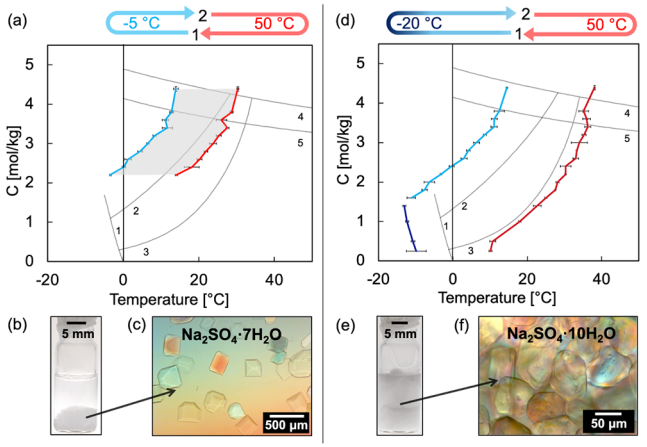

Figure 2. Thermal cycling between −5 and 50 °C (a−c) and −20 and 50 °C (d−f). (a,d) Phase diagram of sodium sulfate (black lines from Steiger and Asmussen: (1) freezing of ice and sodium sulfate decahydrate, solubility lines of (2) sodium sulfate heptahydrate (metastable phase), (3) sodium sulfate decahydrate, (4) thenardite III (metastable phase), and (5) thenardite V) overlaid with our experimental results of the precipitation line of the heptahydrate (light blue) and its dissolution line (red), precipitation of decahydrate and ice (dark blue), and its dissolution (dark red). The shaded area represents the MSZ of the heptahydrate (ΔT = 17 °C). (b,e) Macroscopic image of a 1 mL vial after sodium sulfate heptahydrate precipitation (sodium sulfate decahydrate and ice, respectively). (c,f) Microscopy image of the heptahydrate and decahydrate crystals in the vial, respectively.

precipitated crystals, i.e., plate-like structural shape with angular corners (Figure 2c) under the microscope confirms the heptahydrate form for sodium sulfate as reported in the literature.[20,26]

While heating back to 50 °C, the precipitated heptahydrate crystals in equilibrium with the saturated salt solution dissolve; this is detected by a sharp increase of the transmissivity up to 100%, corresponding to the complete dissolution of the precipitates, and defines the temperature of dissolution at a given concentration, as shown in Figure 2a in red. The experimental dissolution line is very close to the theoretical equilibrium solubility line (+4 °C ± 1 °C beyond). The ΔT between the red and blue line, at a given concentration defines the MSZW, represented by the gray shaded area (Figure 2a), and is found to be constant ($\Delta T \sim 17 \pm 1$ °C) over the concentrations (i.e., parallel to the solubility line). The MSZW represents the region of supersaturation in a solution where spontaneous nucleation is statistically unlikely despite thermodynamic favorability. Classical nucleation theory (CNT) describes nucleation as overcoming a free energy barrier $\Delta G^* = (16\pi\sigma^3)/(3(\Delta\mu)^2)$, where σ is the interfacial crystal/liquid energy and $\Delta\mu$ is the chemical potential difference driving supersaturation ($S > 1$). Below the MSZW, ΔG^* remains high enough that the nucleation rate $J = A \exp(-\Delta G^*/kT)$ is negligible over experimental time scales, even as solute clusters form subcritically.

The very large MSZW obtained during our cooling experiments signals exceptionally slow nucleation kinetics governed by CNT. Ions in aqueous solutions are encased in hydration shells—ordered water molecules tightly bound via electrostatic forces, forming a dynamic barrier.[27,28] Cooling strengthens ion−water interactions, making hydration shells more rigid and ordered as thermal energy decreases, which reduces molecular motion, enhances hydrogen bonding around ions, and hinders crystal embryo formation. This leads to a slight increase in coordination numbers (more water molecules in the first shell) and higher solution viscosity,[29] stabilizing the supersaturated state.[25] Stronger solvation shells at lower temperatures raise the interfacial energy σ. In CNT, high σ elevates the energy barrier ΔG^*, so precritical embryos dissolve rather than grow, allowing large MSZW without phase change. This effect is pronounced in salts with high charge density ions. This large MSZW is problematic for energy storage applications because (i) it introduces a delay in the nucleation cycle and (ii) the hydrate with the highest energy density is not formed. This motivates our search for pathways capable of reducing the MSZW and forming the desired decahydrate salt, mirabilite.

3.1.2. Thermal Cycling between 50 °C and −20 °C. We also perform thermal cycling experiments by cooling far below the freezing point of water, with a reduced minimal temperature of −20 °C, around which ice is expected to form in the salt solution.[15]

Similar to Figure 2a, upon cooling the salt solution from 50 °C, heptahydrate is the first crystal to form, as shown with the precipitation curve (blue) defined in Figure 2d. The cooling steps are subsequently continued down to −20 °C. All the samples extracted at −20 °C are frozen (Figure 2e). However, their Raman spectra (Figure S2) surprisingly show a peak at 989 cm^{-1}, which demonstrates the presence of the decahydrate form, mirabilite, in the bottle rather than the heptahydrate phase. Clearly, mirabilite has been precipitated after the heptahydrate, potentially around the same time as for ice formation. Unfortunately, the instrument used for thermal cycling does not allow us to retrieve the points at which mirabilite precipitates for concentrations above 1.4 mol/kg, since the formation of heptahydrate already attenuates the laser transmissivity down to 0%.

Surprisingly, for concentrations below 1.4 mol/kg, the precipitation of heptahydrate is not even detected prior to mirabilite precipitation. Instead, our results show the direct formation of mirabilite and ice (Figure 2e,f) as shown by the precipitation line in dark blue (Figure 2d), confirmed by Raman analysis. This can be explained by the fact that the precipitation line of heptahydrate is shifted to very low temperatures by the MSZW (ΔT = 17 ± 1 °C) defined earlier.

Lastly, upon heating from −20 to 50 °C, our results reveal a new dissolution line (Figure 2d) that aligns with the predicted solubility line of mirabilite (Figure 2d). This is coherent since, for all the concentrations, we precipitate mirabilite when going to −20 °C, while in the scenario of −5 °C, the precipitation ends at the heptahydrate phase. From these experiments, we can conclude that the dissolution temperature of an unknown crystal at a given concentration on the equilibrium phase diagram with the solubility lines provides a straightforward method to identify which hydrate forms last and remains present in the solution.

3.2. Investigation of the Role of Ice during the Formation of Mirabilite

For concentrations below 1.4 mol/kg, the freezing of the samples below −5 °C, together with the direct formation of mirabilite, poses questions about the role of ice in the formation of mirabilite. Such understanding would aid in finding new ways to directly trigger the nucleation of mirabilite rather than heptahydrate for thermal energy storage.

https://doi.org/10.1021/acs.jpcc.5c08083
J. Phys. Chem. C 2026, 130, 3721−3729

To investigate this, we completed our cycling experiments by carrying out some cooling experiments in a freezer with a window for three concentrations (1.4, 2.8, and 3.8 mol/kg), where we visually track using a camera the bulk salt solution and measure the temperature at the onset of the phase transition precipitation of the three phases (heptahydrate, mirabilite, and ice), as explained in the experimental section.

In several works,[15,17,22] it has been shown that the three phases (heptahydrate, mirabilite, and ice) have different thermal signatures, which can allow one to distinguish them easily. Ice and mirabilite have a rather large latent heat of crystallization (334 kJ/kg[30] and 241 kJ/kg[14] respectively) which leads to large exothermic peaks, while the latent heat of crystallization of the heptahydrate is lower (around 88 kJ/kg), which gives rise to a small bump in a thermal cycle, barely noticeable.

From the thermographs (Figure 3a) for 2.8 and 3.8 mol/kg salt solutions, two distinct peaks of different intensities and

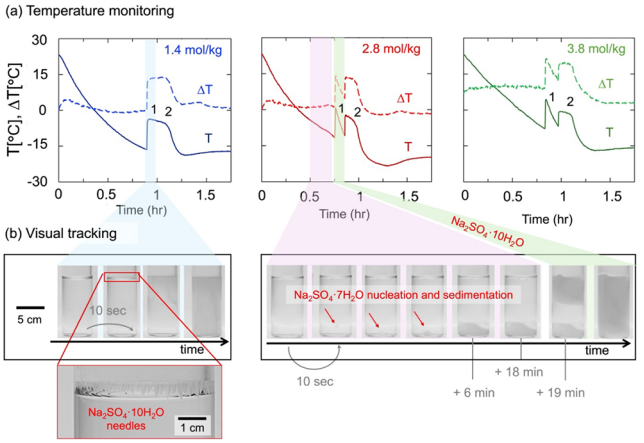

Figure 3. Cooling experiments on sodium sulfate solutions in a freezer. (a) Temperature monitoring for three concentrations of sodium sulfate (1.4, 2.8, and 3.8 mol/kg) in the freezer: temperature vs time (solid line) and $\Delta T = T_{\text{sample}} - T^{\text{ref}}_{\text{ambient freezer}}$ vs time (dashed line). The peaks indexed with number "1" correspond to the nucleation of mirabilite, and number "2" to the formation of ice (highlighted in, e.g., the green and red graphs). The blue, pink, and green shaded areas are to be matched with the colored frames drawn in Figure 3b. (b) Visual tracking for two concentrations of sodium sulfate (1.4 and 2.8 mol/kg) in the freezer. Time between 2 images: 10 s. Not all the images could be shown here, therefore, a jump in time is flagged by the vertical lines on the time-axis.

shapes can be distinguished. Their appearance matches perfectly with the moment at which the samples suddenly turn opaque, as highlighted by the blue and green frames (Figure 3b). Knowing that the integral of ΔT over time is proportional to the latent heat of crystallization, we can deduce that the first peak (smallest integral) corresponds to the mirabilite, as its latent heat is lower than the one of ice, and therefore the second peak (larger integral) corresponds to the ice.

The shape[22] of the two peaks also allows one to distinguish between the two compounds, since the one of ice is large with a plateau, while the one of sodium sulfate decahydrate is narrower and with a concave curvature on the right side. Thus, in these experiments, mirabilite is formed prior to ice and is not ice-assisted.

For the solution at 1.4 mol/kg, the two peaks overlap, although their individual contribution is still noticeable (Figure 3a). This is because, at this concentration, we are much closer to the eutectic composition, i.e., the liquid phase transforms simultaneously into the two solid phases at a constant temperature (theoretical value from the equilibrium phase diagram: 0.42 mol/kg for mirabilite−ice[31]). This reasoning helps to explain the observed correlation between concentration and peak spacing: lower concentrations result in peaks that are closer in time, meaning that the time interval between mirabilite nucleation and ice formation is shorter. For a concentration of 1.4 mol/kg, the ice is forming very quickly after the mirabilite, and the two peaks are almost overlapping.

To further support the macroscopic results obtained in the freezer, we also conduct microscale freezing experiments on a small volume of salt solutions entrapped in microcapillaries placed on a Peltier module as a cooling element, and using a high-speed camera. The progressive steps during cooling and freezing of pure water and a 1.3 mol/kg sodium sulfate solution are represented in Figure 4a and 4b, respectively. For pure water, ice crystallization directly causes the deformation of the liquid/air meniscus of the entrapped droplet. On the other hand, in capillaries containing salt solution, first, the needle-shaped crystals characteristic of mirabilite precipitate at the liquid/air meniscus (Figure 4c). During the growth of the needles of mirabilite, the meniscus maintains its concave curvature, confirming that the growth of the needles is occurring in the liquid surrounding medium. Subsequently, the capillary becomes opaque, and the meniscus deforms, indicating ice formation in a second stage. This microscale experiment provides a second confirmation that mirabilite forms prior to ice during cooling. The full movies of the evolution of the capillaries are available in Supporting Information 1 and 2 and are helpful to visualize two fronts of crystal formation.

3.3. Discussion on the Freezing Experiments and Phase Diagram

For the solution with a concentration of 2.8 mol/kg, bulk crystallization at the bottom of the vial was observed first upon cooling (Figure 3a). Raman spectra of these crystals identify them as the heptahydrate form, which corroborates the results of the thermal cycling. The signature of the heptahydrate is not detected on the thermal graphs, likely due to the little heat generated during its crystallization. Nonetheless, its temperature of precipitation in the freezer (determined by matching with the pictures' sequence) is found to be similar to the one measured by the thermal cycling (Figure 5 light blue points/dashed curve).

Now that we know the order of appearance of all of the phases upon cooling, we can see that the eutectic point of mirabilite and ice is shifted due to this supercooling. Based on our results, we estimate this new eutectic region to be in the range of 1.3−1.4 mol/kg and around −16 ± 3 °C (corresponding to the crossing between the two dark blue lines in Figure 5). For solutions at 2.8 and 3.8 mol/kg upon cooling, as we start forming the heptahydrate phase, the concentration of sodium sulfate available in the solution drops and therefore approaches the eutectic point.

Bednarska et al.[15] argue that mirabilite is not forming from the solution but rather from the transformation of the preexisting heptahydrate through dissolution. They assume that after the heptahydrate formation ice appears and provides

https://doi.org/10.1021/acs.jpcc.5c08083
J. Phys. Chem. C 2026, 130, 3721−3729

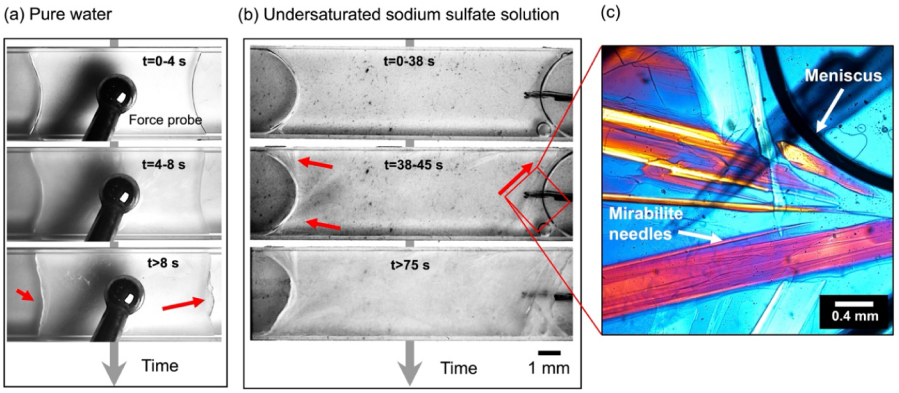

Figure 4. Microscale freezing experiments on microcapillaries cooled with a Peltier element. (a) Freezing of pure water. The red arrows highlight the deformation of the liquid/air meniscus when ice is forming. The cantilever was added to measure the force produced during the formation of ice for another study (not considered in this manuscript). (b) Freezing of an undersaturated solution of sodium sulfate at a concentration of 1.3 mol/kg. The red arrows indicate the formation of mirabilite needles from the liquid/air meniscus. (c) Microscope image in transmission with a cross-polarized filter zooming in on the red rectangle area in (b).

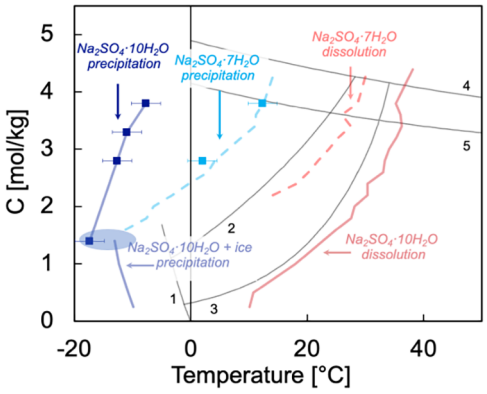

Figure 5. Completed phase diagram of Na_2SO_4−H_2O system with experimental results of the thermal cycling and freezer experiments. Phase diagram of sodium sulfate (black line from Steiger et Asmussen: (1) freezing of ice and sodium sulfate decahydrate, solubility lines of (2) sodium sulfate heptahydrate (metastable phase), (3) sodium sulfate decahydrate, (4) thenardite III (metastable phase), and (5) thenardite V); square points are precipitation temperatures obtained from the freezer experiments of the heptahydrate (light blue) and the decahydrate (dark blue); the rest are results obtained from thermal cycling. Solid lines represent solubility data for mirabilite, and dashed lines represent the heptahydrate. The blue-shaded area represents the eutectic region at the concentration of 1.3−1.4 mol/kg below which the metastability limit of sodium sulfate decahydrate will be at a higher temperature than the one of the heptahydrate phase.

a supersaturation high enough to trigger mirabilite nucleation, and that its growth would be maintained by heptahydrate dissolution. In other words, they affirm that the existence of mirabilite is ice-assisted and requires the presence of heptahydrate.

Our results show that these two conditions are not necessary. Mirabilite can also form before ice precipitation in salt solutions where no prior heptahydrate has appeared. The results and conclusions from the freezer and the Peltier experiments are supported by additional experiments using Differential Scanning Calorimetry (DSC), which are presented in Figure S3.

Figure 5 constitutes a milestone in the understanding of the phase diagram of sodium sulfate upon thermal cycling, as we are reporting the metastability limit (precipitation lines) for the heptahydrate phase and mirabilite, and their MSZW ($\Delta T \sim 17$ °C for heptahydrate and $\Delta T \sim 40$−46 °C for mirabilite). These complementary measurements clarify the events occurring during the cooling of a sodium sulfate solution in the subzero regime and emphasize the need to trigger the nucleation of the stable hydrate artificially to overcome this energy barrier.

3.4. Influence of Additives on Mirabilite Crystallization

Several works have shown that the nucleation of mirabilite is sensitive to impurities present in the sample.[15,17,22,32] In an attempt to promote the precipitation of the decahydrate instead of the heptahydrate without supercooling, we performed additional thermal cycling experiments for a given salt solution (concentration of 2.8 mol/kg) in the presence of impurities that may stimulate the nucleation process through heterogeneous nucleation.

The two current hypotheses to promote mirabilite without supercooling are (1) secondary nucleation[15] (nucleation of mirabilite by virtue of a seed of mirabilite already present in the system) and (2) the use of an isostructural nucleation agent such as *borax* ($Na_2B_4O_7$•$10H_2O$). The presence of the latter in the solution has been shown to facilitate, sometimes but not systematically, mirabilite precipitation upon cooling.[33−35] However, both methods have their disadvantages. In the case of secondary nucleation, it can be difficult to keep some crystals of mirabilite in the solution during thermal cycling. The use of borax, on the other hand, is not optimal either, since it is classified as a *carcinogenic, mutagenic, or toxic* (CMR) substance by the regulation of the European Parliament (REACH) and therefore is not suitable as a sustainable solution for household installations.

We explore heterogeneous nucleation by adding particles with various geometry, size, roughness, and composition to the salt solution prior to cycling (Figure 6a), all with a different lattice spacing compared to sodium sulfate decahydrate. Surprisingly, for all the impurities used, the temperatures of hydrate crystal precipitation ranged between 2.4−6 °C, which matches the temperature range of crystallization of the heptahydrate form (confirmed with Raman spectroscopy, Figure 6b) from pure salt solution. Therefore, none of the impurities are able to promote the formation of mirabilite or reduce the large MSZW, implying that those particles act as poor catalysts for nucleation. Under CNT, the work needed for

https://doi.org/10.1021/acs.jpcc.5c08083
J. Phys. Chem. C 2026, 130, 3721−3729

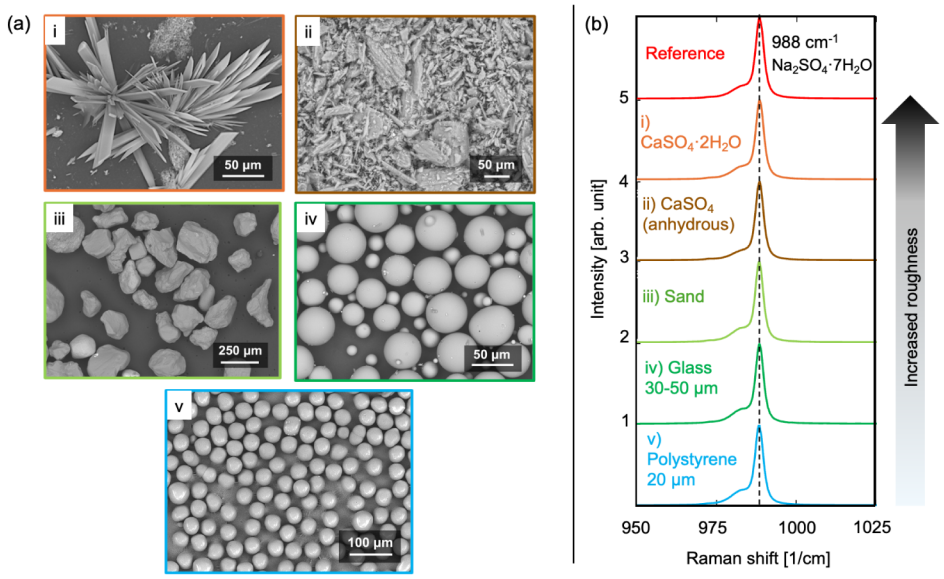

Figure 6. Heterogeneous nucleation from sodium sulfate solution with different types of additives. (a) SEM images of the additives (microparticles) added one by one to the salt solution at C = 2.8 mol/kg (wt. = 0.6%): (i) calcium sulfate dihydrate (gypsum), (ii) calcium sulfate anhydrous, (iii) sand, (iv) glass beads, and (v) polystyrene beads. (b) Raman spectra of the precipitated sodium sulfate crystals under cooling. 988 cm^{-1} is the signature of sodium sulfate heptahydrate crystals, which precipitate in all solutions. Reference = solution without particles. The spectra are offset for the sake of clarity.

heterogeneous nucleation ΔG^*_{het} can be linked to the work for homogeneous nucleation ΔG^*_{homo} with a geometrical function $f(\theta)$ that depends on the contact angle θ between the nucleus and the substrate, the geometry of the nucleus, and interfacial energies: $\Delta G^*_{het} \equiv \Delta G^*_{homo} f(\theta)$, with $0 < f(\theta) \leq 1$.[36] If adding particles does not reduce the MSZW, then the latter has an unfavorable interfacial chemistry/geometry (large θ, poor lattice match, wrong surface charge/functional groups). So, we can consider that when $f(\theta) \approx 1$: they behave almost like "no surface" for that crystal nucleation. Consequently, nucleation remains essentially homogeneous, controlled by bulk supersaturation and the crystal−solution interfacial energy. As said previously, the ionic hydration structure near those particles is "strong enough" or "mismatched enough" that forming a crystal-like embryo on them is not energetically favored. The system, therefore, behaves as if nucleation is controlled by the homogeneous barrier. Although the crystal structure is still thermodynamically preferred at high supersaturation, the path from solution structure to crystal is not catalyzed by those added surfaces.

Perhaps the use of an isostructural template with a smaller structural mismatch could increase the wetting and overcome the nucleation barrier. Since it is very hard to find a nucleating agent that is also not soluble in the solution across the full range of temperatures during thermal cycling, we lastly tried to experiment with micelles using surfactants. The formation of micelles could potentially increase the local concentration of sodium sulfate ions around those micelles and increase the probabilities of ions meeting and pairing up to form the desired salt.

Here, we test two surfactants: cetyltrimethylammonium bromide (CTAB), a positively charged surfactant, and sodium dodecyl sulfate (SDS), a negatively charged surfactant with the same cations as in sodium sulfate. Our results show that CTAB acts more as an inhibitor, and surprisingly avoids all types of crystallization, even the one of the heptahydrate at around 5 °C. Solutions containing SDS are more complicated to study, as the transmissivity drops to 5% around 30 °C due to the formation of micelles. The opacity of the solution makes the detection of sodium sulfate heptahydrate more subtle; however, we could still see a jump in transmissivity down to 0% around 5 °C, which matches with the formation of the heptahydrate seen previously.

In summary, neither heterogeneous nucleation using solid particles nor micellar surfactant impurities facilitated the formation of mirabilite without supercooling. Very recently, the structure of the solvent environment has been recognized to be of utmost importance in the crystallization reaction, even more than the binding of the ions,[37] which could also be a possible explanation for our observations. The understanding of the mechanism underlying the crystallization of sodium sulfate decahydrate remains an open question that warrants further investigation, combining experiments with computational tools that could calculate the energy landscapes of the system at different temperatures. Further techniques of nucleation should be considered, including laser-, pressure-, or ultrasound-induced nucleation, and investigated in more detail to reduce the MSZW and directly form the mirabilite for concentrations above 1.4 mol/kg to optimize its application in thermal energy storage.

4. CONCLUSIONS

Sodium sulfate is a material of interest for thermal battery applications—it has 2 hydrate forms upon cooling, one of which (mirabilite) has a much larger energy density compared to the other (heptahydrate). Here, we extensively study the dynamics of thermal cycling of sodium sulfate solutions over a wide range of concentrations. We experimentally define the metastability limit lines for heptahydrate and decahydrate precipitation. For concentrations above 1.4 mol/kg, heptahydrate is always the first hydrate to precipitate, followed by mirabilite and ice formation when cooling down to −20 °C. At concentrations around 1.4 mol/kg, as the metastability of the

https://doi.org/10.1021/acs.jpcc.5c08083
J. Phys. Chem. C 2026, 130, 3721−3729

heptahydrate passes beyond that of mirabilite, the heptahydrate precipitation is hindered, leading to the direct formation of mirabilite followed by ice crystallization. Precipitation of mirabilite thus occurs directly from the solution without the assistance of ice, regardless of the concentration and the potential amount of heptahydrate formed beforehand. Our data corroborate and complete the existing literature on the phase diagram of sodium sulfate (published after the year 2000) but differ from Hartley et al. (1908)— a gap that could be explained by the lack of precision in controlling the stirring rate and the cooling ramp at their time.

Upon heating, the dissolution lines of the crystals match well with the equilibrium solubility lines of the different phases on the equilibrium phase diagram. Therefore, determining the dissolution temperature at a given concentration for unknown precipitated crystals can serve as a rapid and reliable method to characterize the precipitated material without the use of advanced analytical techniques. It is a complementary technique to Raman and the optical microscope.

For thermal cycling above 0 °C, various additives, including solid particles and micellar structures, are attempted to trigger the nucleation of mirabilite and to reduce its supercooling by heterogeneous nucleation. Our results show that mirabilite cannot be triggered by heterogeneous nucleation in bulk solutions.

Therefore, future research should continue in order to find techniques that can form mirabilite in a controlled manner without any supercooling and without forming the intermediary metastable hydrate, which currently hinders its application for domestic heating.

■ ASSOCIATED CONTENT

Supporting Information

The Supporting Information is available free of charge at https://pubs.acs.org/doi/10.1021/acs.jpcc.5c08083.

Supplementary movies: 1 (freezing of water in capillary) (MP4)

Supplementary movies: 2 (freezing of undersaturated salt solution of sodium sulfate) (MP4)

Experimental conditions choice (Figure S1); Sample characterization: Raman spectra (Figure S2); DSC experiments (Figure S3); Supplementary References (PDF)

■ AUTHOR INFORMATION

Corresponding Author

Noushine Shahidzadeh − *Van der Waals-Zeeman Institute, Institute of Physics, University of Amsterdam, Amsterdam 1098XH, The Netherlands;* orcid.org/0000-0003-2692-0764; Email: n.shahidzadeh@uva.nl

Authors

Anne Claude − *Van der Waals-Zeeman Institute, Institute of Physics, University of Amsterdam, Amsterdam 1098XH, The Netherlands;* orcid.org/0009-0000-7042-6558

Rosa Sinaasappel − *Van der Waals-Zeeman Institute, Institute of Physics, University of Amsterdam, Amsterdam 1098XH, The Netherlands*

Jorik van de Groep − *Van der Waals-Zeeman Institute, Institute of Physics, University of Amsterdam, Amsterdam 1098XH, The Netherlands;* orcid.org/0000-0003-3033-8005

Complete contact information is available at: https://pubs.acs.org/10.1021/acs.jpcc.5c08083

Author Contributions

R.S. performed the microcapillaries experiments. A.C. carried out the experiments of thermal cycling and freezer, and combined and analyzed the results. A.C., N.S., JvdG developed the idea, designed the experiments, and wrote the manuscript.

Notes

The authors declare no competing financial interest.

■ ACKNOWLEDGMENTS

The authors thank the Institute of Physics at the University of Amsterdam for the financial support. We acknowledge AMOLF (The Netherlands) for the DSC experiments and Technobis for kindly lending the Crystal16® machine. This work was funded by institutional funding of the Institute of Physics at the University of Amsterdam.

■ REFERENCES

(1) IEA. *Shares of residential energy consumption by end use in selected IEA countries, 2018*. https://www.iea.org/data-and-statistics/charts/shares-of-residential-energy-consumption-by-end-use-in-selected-iea-countries-2018.

(2) IEA *Buildings-related energy demand for heating and share by fuel in the Net Zero Scenario, 2022−2030*. https://www.iea.org/data-and-statistics/charts/buildings-related-energy-demand-for-heating-and-share-by-fuel-in-the-net-zero-scenario-2022-2030.

(3) European Union. *Regulation (EU) 2021/1119 of the European Parliament and of the Council of 30 June 2021 Establishing the Framework for Achieving Climate Neutrality and Amending Regulations (EC) No 401/2009 and (EU) 2018/1999 ('European Climate Law')*; European Union, 2021.

(4) Farid, M. M.; Khudhair, A. M.; Razack, S. A. K.; Al-Hallaj, S. A review on phase change energy storage: materials and applications. *Energy Convers. Manag.* **2004**, *45*, 1597−1615.

(5) Lane, G. A. Phase change materials for energy storage nucleation to prevent supercooling. *Sol. Energy Mater. Sol. Cells* **1992**, *27*, 135−160.

(6) Sögütoglu, L. C.; Donkers, P. A. J.; Fischer, H. R.; Huinink, H. P.; Adan, O. C. G. In-depth investigation of thermochemical performance in a heat battery: Cyclic analysis of K2CO3, MgCl2 and Na2S. *Appl. Energy* **2018**, *215*, 159−173.

(7) Spietz, T.; Fryza, R.; Lasek, J.; Zuwała, J. Thermochemical Energy Storage Based on Salt Hydrates: A Comprehensive Review. *Energies* **2025**, *18*, 2643.

(8) Shkatulov, A.; Joosten, R.; Fischer, H.; Huinink, H. Core−Shell Encapsulation of Salt Hydrates into Mesoporous Silica Shells for Thermochemical Energy Storage. *ACS Appl. Energy Mater.* **2020**, *3*, 6860−6869.

(9) Manthiram, A. An Outlook on Lithium Ion Battery Technology. *ACS Cent. Sci* **2017**, *3*, 1063−1069.

(10) Fang, H. Challenges with the Ultimate Energy Density with Li-ion Batteries. *IOP Conf. Ser. Earth Environ. Sci.* **2021**, *781*, 042023.

(11) Pierie, F.; van Someren, C. *Energy Storage Label: A Method for Comparing Storage Systems over All Ranges*; Hanzehogeschool Groningen. 2015.

(12) Marliacy, P.; Solimando, R.; Bouroukba, M.; Schuffenecker, L. Thermodynamics of crystallization of sodium sulfate decahydrate in H2O−NaCl−Na2SO4: application to Na2SO4·10H2O-based latent heat storage materials. *Thermochim. Acta* **2000**, *344*, 85−94.

(13) Madhlopa, A. Chapter 6 - Concepts of thermal energy storage and solar receivers. in *Solar Receivers for Thermal Power Generation*; Academic Press, 2022, pp. 151−189.DOI: .

(14) Sharma, A.; Tyagi, V. V.; Chen, C. R.; Buddhi, D. Review on thermal energy storage with phase change materials and applications. *Renew. Sustain. Energy Rev.* **2009**, *13*, 318−345.
(15) Bednarska, D.; Koniorczyk, M.; Steiger, M. Identification of various salt crystallization and water freezing patterns induced by temperature variation from Na2SO4 − H2O system confined in porous materials. *Constr. Build. Mater.* **2022**, *347*, 128540.
(16) Steiger, M.; Asmussen, S. Crystallization of sodium sulfate phases in porous materials: The phase diagram Na2SO4−H2O and the generation of stress. *Geochim. Cosmochim. Acta* **2008**, *72*, 4291−4306.
(17) Espinosa-Marzal, R.; Scherer, G. Crystallization of sodium sulfate salts in limestone. *Environ. Geol.* **2008**, *56*, 605.
(18) Derluyn, H.; Saidov, T. A.; Espinosa-Marzal, R. M.; Pel, L.; Scherer, G. W. Sodium sulfate heptahydrate I: The growth of single crystals. *J. Cryst. Growth* **2011**, *329*, 44−51.
(19) Bracciale, M. P.; Sammut, S.; Cassar, J.; Santarelli, M. L.; Marrocchi, A. Molecular Crystallization Inhibitors for Salt Damage Control in Porous Materials: An Overview. *Molecules* **2020**, *25*, 1873.
(20) Hamilton, A.; Hall, C.; Pel, L. Sodium sulfate heptahydrate: direct observation of crystallization in a porous material. *J. Phys. Appl. Phys.* **2008**, *41*, 212002.
(21) Hartley, H.; Jones, B.M.; Hutchinson, G.A. LXXV.—The spontaneous crystallisation of sodium sulphate solutions. *J. Chem. Soc., Trans* **1908**, *93*, 825−833.
(22) Denecker, M. F. C.; Hebert, R. L.; Wassermann, J.; Dosseh, G.; Menendez, B.; Bourgès, A. Experimental study of the crystallization of sodium sulfate hydrates through temperature monitoring. *Environ. Earth Sci.* **2014**, *72*, 5089−5099.
(23) Balarew, C.; Tepavitcharova, S.; Kamburov, S. Study of the spontaneous crystallization of $Na_2SO_4{\cdot}7H_2O$ and $Na_2SeO_4{\cdot}7.5H_2O$. *Monatsh. Chem.* **2017**, *149*, 289−298.
(24) Ulrich, J.; Strege, C. Some aspects of the importance of metastable zone width and nucleation in industrial crystallizers. *J. Cryst. Growth* **2002**, *237*−*239*, 2130−2135.
(25) Kadam, S. S.; Kulkarni, S. A.; Ribera, R. C.; Stankiewicz, A. I.; Horst, J. H. T.; Kramer, H. J. M. A new view on the metastable zone width during cooling crystallization. *Chem. Eng. Sci.* **2012**, *72*, 10−19.
(26) Denecker, M. *Le rôle des sulfates de sodium dans l'altération des pierres du patrimoine bâti: méthodes indirectes d'identification pour l'approche expérimentale*; HAL, 2015.
(27) Gao, Z.; Teleanu, F.; Marr, K. A.; Jerschow, A. Molecular Shells and Range of Interactions in Ionic Liquids as a Function of Temperature. *J. Phys. Chem. Lett.* **2025**, *16*, 2120−2127.
(28) Bian, C.; Chen, H.; Song, X.; Yu, J. Metastable zone width and the primary nucleation kinetics for cooling crystallization of NaNO3 from NaCl-NaNO3-H2O system. *J. Cryst. Growth* **2019**, *518*, 5−13.
(29) Ozbek, H.; Fair, J. A.; Phillips, S. L. Viscosity of Aqueous Sodium Chloride Solutions From 0 - 150° C. *American Chemical Society 29th Southeast Regional Meeting*, UNT, https://digital.library.unt.edu/ark:/67531/metadc1014165/. 1977.
(30) Kumano, H.; Asaoka, T.; Saito, A.; Okawa, S. Study on latent heat of fusion of ice in aqueous solutions. *Int. J. Refrig.* **2007**, *30*, 267−273.
(31) Brand, H. E. A.; Fortes, A. D.; Wood, I. G.; Knight, K. S.; Vočadlo, L. The thermal expansion and crystal structure of mirabilite (Na2SO4·10D2O) from 4.2 to 300 K, determined by time-of-flight neutron powder diffraction. *Phys. Chem. Miner.* **2009**, *36*, 29−46.
(32) Khaleghi Dehghan, A.; Manteghian, M. SiC-added particles triggering effect in nucleation of Glauber hydrate salt. *J. Mater. Res.* **2023**, *38*, 4913−4926.
(33) Telkes, M. Nucleation of Supersaturated Inorganic Salt Solutions. *Ind. Eng. Chem.* **1952**, *44*, 1308−1310.
(34) Goswami, M.; Kumar, N.; Li, Y.; Hirschey, J.; La Clair, T. J.; Akamo, D. O.; Sultan, S.; Rios, O.; Gluesenkamp, K. R.; Graham, S. Understanding supercooling mechanism in sodium sulfate decahydrate phase-change material. *J. Appl. Phys.* **2021**, *129*, 245109.
(35) Levy, H. A.; Lisensky, G. C. Crystal structures of sodium sulfate decahydrate (Glauber's salt) and sodium tetraborate decahydrate (borax). Redetermination by neutron diffraction. *Acta Crystallogr. B* **1978**, *34*, 3502−3510.
(36) Rudolph, P. *Crystal Growth Fundamentals: thermodynamics of Crystallization.*; De Gruyter, 2025. DOI: 10.1515/9783111711164.
(37) Martin, J. D. Solutes don't crystallize! Insights from phase diagrams demystify the "magic" of crystallization. *Matter* **2024**, *7*, 3290−3316.